



Synthesis and antiseizure activity of (*E*)-1,2-diarylethylidenehydrazine carboximidamides against tonic-clonic seizures: an intracerebroventricular and electrophysiological study

Fariba Abedi Firouzjaei¹ · Elmira Heidarli² · Shabnam Ravan² · Sayed Masoud Hosseini² · Nima Naderi² · Kiarash Almasyan³ · Afshin Sarvary¹ · Hamid Irannejad^{3,4}

Received: 5 January 2020 / Accepted: 27 May 2020
© Springer Science+Business Media, LLC, part of Springer Nature 2020

Abstract

A series of (*E*)-1,2-diarylethylidenehydrazine carboximidamides **2a–j** were synthesized and characterized by NOESY experiment as anticonvulsant agents and their antiseizure activity was evaluated by intracerebroventricular administration of compounds. Most of the compounds had significant protection against tonic-clonic seizures and **2a** was found to be as equipotent as carbamazepine in seizures control. In order to find their anticonvulsant mechanism of action, **2a** was subjected to further electrophysiological studies using patch-clamp technique. The results confirmed that this compound is neither a voltage-gated sodium channel blocker nor a NMDA/AMPA antagonist. Although **2a** did not show any direct GABA agonistic activity, it could decrease EPSP and increase IPSP frequency without any change in amplitude. Finally, the results indicated most likely a presynaptic GABA-mediated mechanism of **2a** for its antiseizure activity such as inhibition of the GABA-T which was validated by molecular docking.

Keywords Epilepsy · Hydrazinecarboximidamide · Intracerebroventricular · Patch-clamp · Tonic-clonic seizures · GABA-T

Introduction

Epilepsy is a chronic cerebral disorder characterized by partial or generalized seizures of the body. Seizures are due to successive electrical discharges of neurons which tend to unintentional body movements. Approximately, 50 million people

in the world live with epilepsy and 70% of epileptic patients respond to antiepileptic drugs (AED). AEDs may cause adverse effects which are common among patients receiving medicines and can have a considerable impact on quality of life, contributing to failure of treatment. The most common side effects of AEDs include dizziness, nausea, headache, vomiting, fatigue, vertigo, ataxia and blurred vision, and so on which are a motivation for drug discontinuation in 40% of cases. Therefore, the emerge of further research to develop novel AEDs with fewer side effects and higher effectiveness is of great importance (Perucca and Meador 2005).

Owing to the complex mechanisms involved in seizures, structurally various AEDs with different mechanisms have been discovered and introduced. Among compounds classes, carbazides and carbazones are an interesting scaffold for consideration in AED structures due to their hydrogen bonding potential, because hydrogen bonding domain is a main part of pharmacophoric elements of AEDs. More specifically, hydrazinecarboxamides and hydrazinecarbothioamides have prominent and various biological and pharmacological activities like trypanocidal, cathepsin L (Compound **I** in Fig. 1) and tyrosinase inhibition (Compound **II**) (Fatondji et al. 2013; Haldys et al. 2018; Kumar et al. 2010; Song et al. 2017). Moreover, anti-retroviral activity of thiosemicarbazone metal complexes against

Supplementary information The online version of this article (<https://doi.org/10.1007/s00044-020-02576-7>) contains supplementary material, which is available to authorized users.

✉ Nima Naderi
naderi@sbmu.ac.ir
✉ Hamid Irannejad
irannejadhamid@gmail.com

¹ Department of Chemistry, Faculty of Science, Babol Noshirvani University of Technology, Babol, Iran
² Department of Pharmacology & Toxicology, School of Pharmacy, Shahid Beheshti University of Medical Sciences, Tehran, Iran
³ Department of Medicinal Chemistry, Faculty of Pharmacy, Mazandaran University of Medical Sciences, Sari, Iran
⁴ Pharmaceutical Sciences Research Center, Mazandaran University of Medical Sciences, Sari, Iran

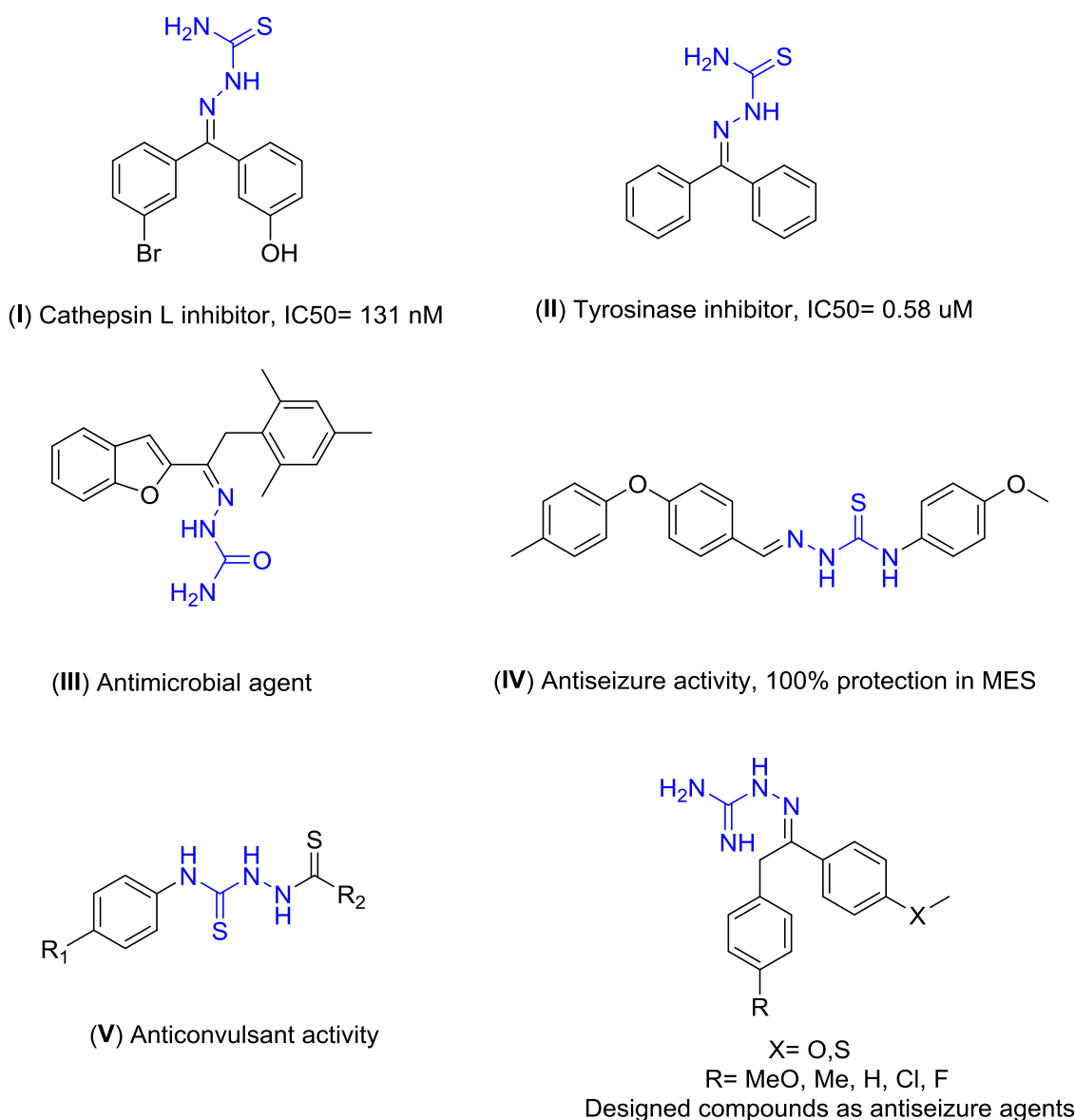


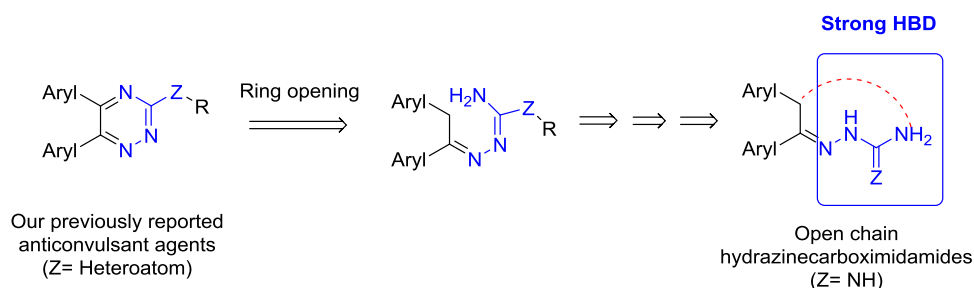
Fig. 1 Structures of some semicarbazone/thiosemicarbazone derivatives reported in literature as active pharmacological agents and the structure of newly designed compounds

HIV-1 and HTLV-1 has been studied and reported by Pelosi et al. (2010). Recently, Urease inhibition activity has been reported for some benzophenone semicarbazone/thiosemicarbazone derivatives (Compound III) and also thiosemicarbazide derivatives have displayed antibacterial and antiproliferative effects (Arshia et al. 2016; Pitucha et al. 2016). Above all, hydrazinecarbothioamides IV and V have been reported several times in literature as anticonvulsant agents (Nevagi et al. 2014; Shafiee et al. 2009; Tripathi and Kumar 2013).

In this study, some hydrazinecarboximidamides (Fig. 1) were designed and synthesized by conventional methods and their correct structures were confirmed by NMR and Mass spectra. Designing was based on our previously reported anticonvulsant agents with 5,6-diaryl-1,2,4-triazine structure

(Irannejad et al. 2014; Irannejad et al. 2015). In order to have a highly potential hydrogen bonding domain which is a requisite pharmacophoric element in anticonvulsant agents, 1,2,4-triazine ring was considered to be in the form of an open chain to confer more flexibility and hydrogen bonding capability (Fig. 2). In this case, hydrazone moiety can exist in two geometrical isomeric forms *E/Z* which were characterized by NOESY experiment and compared with the previously reported similar compounds. Subsequently, their antiseizure activity was evaluated by intracerebroventricular (i.c.v.) injection of compounds against seizures induced by subcutaneous (s.c) injection of pentylenetetrazole (PTZ) and their mechanism of antiseizure activity was studied by voltage and current-clamp method on DG hippocampal neuron cells.

Fig. 2 The strategy of designing open chain hydrazinecarboximidamides by ring opening of our previously reported 5,6-diaryl-1,2,4-triazine anticonvulsant agents



Methods and materials

All chemical reagents and solvents were purchased from Sigma–Aldrich or Merck suppliers and used without further purification. The progress of reactions was checked by thin-layer chromatography (TLC) by using TLC Silica gel 60 F₂₅₄ (Merck, Darmstadt, Germany). UV cabinet with wavelengths 254 and 360 nm was used for visualizing spots on TLC. Column chromatography was performed by Silica gel 60 (0.040–0.063 mm), Merck, Germany. Melting points were measured in open capillaries on a Stuart Scientific apparatus and are uncorrected. IR spectra were recorded on a FT-IR Perkin Elmer spectrometer. NMR spectra were recorded on Bruker 400 MHz (Germany) and tetramethylsilane was used as standard and chemical shifts are expressed in ppm units. Coupling constants are reported in Hertz (Hz). Low resolution mass spectra were measured using a HP 5975 Mass Selective Detector (Agilent technologies, USA). Elemental analyses for C, H, and N were performed by using a CHN elemental analyzer (GmbH-Germany), and the results are within $\pm 0.4\%$ of the theoretical values.

General procedure

Synthesis of 1,2-Diarylethanones (1a–j)

To a mixture of arylacetic acid derivatives (1 eq), anisole or thioanisole (1.2 eq) and phosphoric acid (1.2 eq), was added trifluoroacetic anhydride (4 eq) and the resulting mixture was stirred at room temperature for 10 min. Crushed ice was added to the mixture to precipitate the product and then it was filtered and washed with water and petroleum ether. It was used in the next step without further purification. Compounds characterization was previously reported by us in our recent publication (Kucukkilinc et al. 2017; Valipour et al. 2019).

Synthesis of (E)-1,2-Diarylethylidenecarboximidamides (2a–j)

To a suspension of 1,2-diarylethanones (1a–j) (1 eq) in 2-propanol, was added aminoguanidine (1.5 eq) and

catalytic amounts of hydrochloric acid (37%) and the mixture was refluxed for 24 h to complete the reaction monitored by TLC. After completion of reaction, it was cooled to room temperature to precipitate the product, then filtered off and washed by water. If necessary, recrystallization was performed in 2-propanol to give the pure product.

(E)-2-(2-(4-methoxyphenyl)-1-(4-(methylthio)phenyl)ethylidene) hydrazinecarboximidamide (2a)

White powder (0.21 g, yield 35%); mp 231–233 °C. IR (KBr) (ν_{\max} /cm⁻¹): 3455, 3061, 2989, 1684, 1622, 1513, 1439, 1246, 1030, 830. ¹H-NMR (400 MHz, DMSO-*d*₆): δ_{H} (ppm) 2.46 (3H, *s*, SCH₃), 3.67 (3H, *s*, OCH₃), 4.24 (2H, *s*, CH₂), 6.83 (2H, *d*, ³*J*_{HH} = 8.6 Hz, H–Ar), 7.10 (2H, *d*, ³*J*_{HH} = 8.6 Hz, H–Ar), 7.21 (2H, *d*, ³*J*_{HH} = 8.5 Hz, H–Ar), 7.80 (3H, *brs*, NH and NH₂), 7.91 (2H, *d*, ³*J*_{HH} = 8.5 Hz, H–Ar), 11.64 (1H, *brs*, NH). ¹³C-NMR (100 MHz, DMSO-*d*₆) δ_{C} (ppm) 14.2 (SCH₃), 31.3 (CH₂), 55.0 (OCH₃), 114.1, 125.1, 127.2, 127.7, 129.3, 132.2, 140.5, 152.5, 156.1, 157.9. EI-MS, *m/z* (%): 328 (M⁺, 15), 243(20), 151(50), 109(100), 80(30), 45(60). Anal. Calcd for C₁₇H₂₀N₄OS: C, 62.17; H, 6.14; N, 17.06. Found: C, 62.21; H, 4.16; N, 17.11.

(E)-2-(1-(4-(methylthio)phenyl)-2-(*p*-tolyl)ethylidene) hydrazinecarboximidamide (2b)

White powder (0.32 g, yield 53%); mp 236–238 °C. IR (KBr) (ν_{\max} /cm⁻¹): 3465, 3269, 1682, 1621, 1495, 1318, 1140, 988, 761. ¹H-NMR (400 MHz, DMSO-*d*₆): δ_{H} (ppm) 2.20 (3H, *s*, CH₃), 2.46 (3H, *s*, SCH₃), 4.27 (2H, *s*, CH₂), 7.06 (4H, *s*, H–Ar), 7.20 (2H, *d*, ³*J*_{HH} = 8.5 Hz, H–Ar), 7.85 (3H, *brs*, NH and NH₂), 7.90 (2H, *d*, ³*J*_{HH} = 8.5 Hz, H–Ar), 11.69 (1H, *brs*, NH). ¹³C-NMR (100 MHz, DMSO-*d*₆) δ_{C} (ppm) 14.1 (SCH₃), 20.5 (CH₃), 31.8 (CH₂), 125.0, 127.7, 128.1, 129.2, 132.2, 132.4, 135.6, 140.5, 152.3, 156.1. EI-MS, *m/z* (%): 312 (M⁺, 10), 207 (21), 151(50), 109(72), 81(20), 44(100). Anal. Calcd for C₁₇H₂₀N₄S: C, 65.35; H, 6.45; N, 17.93. Found: C, 65.42; H, 6.43; N, 17.98.

(E)-2-(1-(4-(methylthio)phenyl)-2-phenylethylidene)hydrazinecarboximidamide (2c)

White powder (0.46 g, yield 75%); mp 218–220 °C. IR (KBr) (ν_{\max} /cm⁻¹): 3465, 3152, 2989, 1689, 1623, 1495, 1322, 1095, 739. ¹H-NMR (400 MHz, DMSO-*d*₆): δ_{H} (ppm) 2.46 (3H, *s*, SCH₃), 4.33 (2H, *s*, CH₂), 7.18–7.29 (7H, *m*, H–Ar), 7.85 (3H, *brs*, NH and NH₂), 7.91 (2H, *d*, ³*J*_{HH} = 8.50 Hz, H–Ar), 11.66 (1H, *brs*, NH). ¹³C-NMR (100 MHz, DMSO-*d*₆) δ_{C} (ppm) 14.1 (SCH₃), 32.2 (CH₂), 125.1, 126.5, 127.6, 128.2, 128.7, 132.2, 135.5, 140.5, 152.1, 156.1. EI-MS, *m/z* (%): 298(M⁺, 95), 224 (60), 207 (58), 151(60), 109(90), 91 (30), 45 (100). Anal. Calcd for C₁₆H₂₁N₄S: C, 64.40; H, 6.08; N, 18.78. Found: C, 64.32; H, 6.11; N, 18.84.

(E)-2-(2-(4-chlorophenyl)-1-(4-(methylthio)phenyl)ethylidene)hydrazinecarboximidamide (2d)

White powder (0.09 g, yield 77%); mp 250–252 °C. IR (KBr) (ν_{\max} /cm⁻¹): 3466, 3265, 2920, 1685, 1623, 1493, 1435, 1094, 1014, 821. ¹H-NMR (300 MHz, DMSO-*d*₆): δ_{H} (ppm) 2.47 (3H, *s*, SCH₃), 4.34 (2H, *s*, CH₂), 7.20 (2H, *d*, ³*J*_{HH} = 8.4 Hz, H–Ar), 7.22 (2H, *d*, ³*J*_{HH} = 8.4 Hz, H–Ar), 7.34 (2H, *d*, ³*J*_{HH} = 8.40 Hz, H–Ar), 7.80 (3H, *brs*, NH and NH₂), 7.91 (2H, *d*, ³*J*_{HH} = 8.40 Hz), 11.70 (1H, *brs*, NH). ¹³C-NMR (75 MHz, DMSO-*d*₆) δ_{C} (ppm) 14.5 (SCH₃), 31.3 (CH₂), 125.5, 128.1, 129.1, 130.5, 131.7, 132.3, 135.1, 141.2, 152.1, 156.5. EI-MS, *m/z* (%): 332 (M⁺, 9), 275 (9), 207 (16), 151 (43), 109 (81), 44 (100). Anal. Calcd for C₁₆H₁₇ClN₄S: C, 57.74; H, 5.15; N, 16.83. Found: C, 57.81; H, 5.18; N, 16.75.

(E)-2-(2-(4-fluorophenyl)-1-(4-(methylthio)phenyl)ethylidene)hydrazinecarboximidamide (2e)

White powder (0.19 g, yield 70%); mp 253–255 °C. IR (KBr) (ν_{\max} /cm⁻¹): 3469, 30264, 1686, 1622, 1600, 1508, 1324, 1221, 1096, 822. ¹H-NMR (400 MHz, DMSO-*d*₆): δ_{H} (ppm) 2.47 (3H, *s*, SCH₃), 4.33 (2H, *s*, CH₂), 7.10 (2H, *t*, ³*J*_{HH} = 8.7 Hz, H–Ar), 7.20–7.24 (4H, *m*, H–Ar), 7.89 (3H, *brs*, NH and NH₂), 7.91 (2H, *d*, ³*J*_{HH} = 8.5 Hz, H–Ar), 11.76 (1H, *brs*, NH). ¹³C-NMR (100 MHz, DMSO-*d*₆) δ_{C} (ppm) 14.1 (SCH₃), 31.3 (CH₂), 115.5 (*d*, ²*J*_{CF} = 21.10 Hz), 125.1, 127.7, 130.1 (*d*, ³*J*_{CF} = 7.9 Hz), 131.7 (*d*, ⁴*J*_{CF} = 3.0 Hz), 132.0, 140.7, 152.0, 156.1, 161.0 (*d*, ¹*J*_{CF} = 241.1 Hz). EI-MS, *m/z* (%): 303 (20), 272(40), 224 (24), 183(20), 151 (22), 134 (29), 44(100). Anal. Calcd for C₁₆H₁₇FN₄S: C, 60.74; H, 5.42; N, 17.71. Found: C, 60.64; H, 5.49; N, 17.77.

(E)-2-(1,2-bis(4-methoxyphenyl)ethylidene)hydrazinecarboximidamide (2f)

White powder (0.55 g, yield 91%); mp 233–240 °C. IR (KBr) (ν_{\max} /cm⁻¹): 3421, 3150, 2936, 1660, 1511, 1464,

1260, 1026, 810. ¹H-NMR (400 MHz, DMSO-*d*₆): δ_{H} (ppm) 3.67 (3H, *s*, OCH₃), 3.76 (3H, *s*, OCH₃), 4.23 (2H, *s*, CH₂), 6.83 (2H, *d*, ³*J*_{HH} = 8.6 Hz, H–Ar), 6.90 (2H, *d*, ³*J*_{HH} = 8.9 Hz, H–Ar), 7.10 (2H, *d*, ³*J*_{HH} = 8.6 Hz, H–Ar), 7.85 (3H, *brs*, NH and NH₂), 7.92 (2H, *d*, ³*J*_{HH} = 8.9 Hz, H–Ar), 11.55 (1H, *brs*, NH). ¹³C-NMR (100 MHz, DMSO-*d*₆) δ_{C} (ppm) 31.4 (CH₂), 55.0 (OCH₃), 55.2 (OCH₃), 113.6, 114.1, 127.3, 128.3, 128.9, 129.3, 152.7, 156.0, 157.9, 160.4. EI-MS, *m/z* (%): 312 (M⁺, 100), 238 (88), 229 (95), 191 (91), 149 (75), 121 (80), 104 (65), 77 (79). Anal. Calcd for C₁₇H₂₀N₄O₂: C, 65.37; H, 6.45; N, 17.94. Found: C, 65.46; H, 6.49; N, 17.88.

(E)-2-(1-(4-methoxyphenyl)-2-(*p*-tolyl)ethylidene)hydrazinecarboximidamide (2g)

White powder (0.52 g, yield 85%); mp 218–220 °C. IR (KBr) (ν_{\max} /cm⁻¹): 3425, 3255, 2933, 1595, 1517, 1513, 1463, 1260, 1027, 846. ¹H-NMR (400 MHz, DMSO-*d*₆): δ_{H} (ppm) 2.21 (3H, *s*, CH₃), 3.75 (3H, *s*, OCH₃), 4.25 (2H, *s*, CH₂), 6.90 (2H, *d*, ³*J*_{HH} = 8.9 Hz, H–Ar), 7.06 (4H, *s*, H–Ar), 7.84 (3H, *brs*, NH and NH₂), 7.91 (2H, *d*, ³*J*_{HH} = 8.9 Hz, H–Ar), 11.55 (1H, *brs*, NH). ¹³C-NMR (100 MHz, DMSO-*d*₆) δ_{C} (ppm) 20.5 (CH₃), 31.9 (CH₂), 55.2 (OCH₃), 113.6, 128.1, 128.3, 128.8, 129.2, 132.5, 135.5, 152.5, 156.0, 160.4. EI-MS, *m/z* (%): 296 (M⁺, 96), 237 (34), 222 (87), 191 (100), 149 (74), 134 (74), 105 (46). Anal. Calcd for C₁₇H₂₀N₄O: C, 68.90; H, 6.80; N, 18.90. Found: C, 68.81; H, 6.88; N, 18.98.

(E)-2-(1-(4-methoxyphenyl)-2-phenylethylidene)hydrazinecarboximidamide (2h)

White powder (0.35 g, yield 57%); mp 188–190 °C. IR (KBr) (ν_{\max} /cm⁻¹): 3464, 3262, 2836, 1684, 1619, 1513, 1253, 1028, 838. ¹H-NMR (400 MHz, DMSO-*d*₆): δ_{H} (ppm) 3.75 (3H, *s*, OCH₃), 4.31 (2H, *s*, CH₂), 6.90 (2H, *d*, ³*J*_{HH} = 8.9 Hz, H–Ar), 7.16–7.29 (5H, *m*, H–Ar), 7.84 (3H, *brs*, NH and NH₂), 7.92 (2H, *d*, ³*J*_{HH} = 8.9 Hz, H–Ar), 11.55 (1H, *brs*, NH). ¹³C-NMR (100 MHz, DMSO-*d*₆) δ_{C} (ppm) 32.3 (CH₂), 55.2 (OCH₃), 113.7, 126.5, 128.2, 128.3, 128.7, 128.8, 135.7, 152.3, 156.0, 160.5. EI-MS, *m/z* (%): 282 (M⁺, 100), 223 (24), 208 (64), 191 (88), 165 (24), 149 (65), 134 (29), 91 (31). Anal. Calcd for C₁₆H₁₈N₄O: C, 68.06; H, 6.43; N, 19.84. Found: C, 68.19; H, 6.40; N, 19.79.

(E)-2-(2-(4-chlorophenyl)-1-(4-methoxyphenyl)ethylidene)hydrazinecarboximidamide (2i)

White powder (0.54 g, yield 89%); mp 222–224 °C. IR (KBr) (ν_{\max} /cm⁻¹): 3461, 2952, 2559, 1688, 1569, 1492, 1305, 845. ¹H-NMR (400 MHz, DMSO-*d*₆): δ_{H} (ppm) 3.76 (3H, *s*, OCH₃), 4.32 (2H, *s*, CH₂), 6.91 (2H, *d*, ³*J*_{HH} =

8.8 Hz, H–Ar), 7.21 (2H, *d*, $^3J_{\text{HH}} = 8.3$ Hz, H–Ar), 7.33 (2H, *d*, $^3J_{\text{HH}} = 8.3$ Hz, H–Ar), 7.80 (3H, brs, NH and NH₂), 7.91 (2H, *d*, $^3J_{\text{HH}} = 8.8$ Hz, H–Ar), 11.63 (1H, brs, NH). ¹³C-NMR (100 MHz, DMSO-*d*₆) δ_{C} (ppm) 31.6 (CH₂), 55.2 (OCH₃), 113.7, 128.1, 128.6, 128.8, 130.1, 131.1, 134.8, 151.8, 156.1, 160.5. EI-MS, *m/z* (%): 314 (17), 281 (11), 238 (9), 218 (24), 135 (100), 103 (34), 77 (45). Anal. Calcd for C₁₆H₁₇ClN₄O: C, 60.66; H, 5.41; N, 17.69. Found: C, 60.75; H, 5.44; N, 17.76.

(E)-2-(2-(4-fluorophenyl)-1-(4-methoxyphenyl)ethylidene)hydrazinecarboximidamide (2j)

White powder (0.21 g, yield 34%); mp 190–192 °C. IR (KBr) (ν_{max} /cm^{−1}): 3466, 3274, 2837, 1689, 1570, 1510, 1181, 1028, 1030, 831. ¹H-NMR (400 MHz, DMSO-*d*₆): δ_{H} (ppm) 3.75 (3H, *s*, OCH₃), 4.30 (2H, *s*, CH₂), 6.90 (2H, *d*, $^3J_{\text{HH}} = 8.8$ Hz, H–Ar), 7.09 (2H, *t*, $^3J_{\text{HH}} = 8.7$ Hz, H–Ar), 7.21 (2H, *dd*, $^3J_{\text{HH}} = 8.5$, 5.5 Hz, H–Ar), 7.72 (3H, brs, NH and NH₂), 7.91 (2H, *d*, $^3J_{\text{HH}} = 8.8$ Hz, H–Ar), 11.60 (1H, brs, NH). ¹³C-NMR (100 MHz, DMSO-*d*₆) δ_{C} (ppm) 31.4 (CH₂), 55.3 (OCH₃), 113.7, 115.4 (*d*, $^2J_{\text{CF}} = 21.1$ Hz), 128.3, 128.8, 130.2 (*d*, $^3J_{\text{CF}} = 7.90$ Hz), 132.0, 152.2, 156.4, 160.5, 161.0 (*d*, $^1J_{\text{CF}} = 240.9$ Hz). EI-MS, *m/z* (%): 300 (M⁺, 100), 241 (28), 226 (68), 191 (93), 149 (65), 134 (71), 109 (61). Anal. Calcd for C₁₆H₁₇FN₄O: C, 63.99; H, 5.71; N, 18.66. Found: C, 63.87; H, 5.76; N, 18.74.

Pharmacology

The antiseizure effects of the test compounds were evaluated using PTZ-induced seizure in rats. Male wistar rats (150–200 g; Pasteur Institute, Tehran, Iran) were used in this study. They were kept in animal facility with free access to food and water and were housed on a 12/12 h light/dark cycle (lights on at 7:00 a.m.), and temperature of 23 ± 2 °C. Efforts were made to minimize the number of animals in each group. Animal care and experimental procedures were in accordance with Iranian Ministry of Health and Medical Education Guidelines and were approved by University Ethics Committee (approval No. IR.SBMU.PHNM.1395.543).

Stereotaxic surgery and drug administration

Rats were anesthetized by intraperitoneal injection of ketamine (100 mg/kg) and xylazine (10 mg/kg) and were placed in a stereotaxic surgery device (Stoelting, IL, USA). A 23-gauge stainless-steel cannula was implanted 1 mm above the left lateral ventricle (at the following coordinates with reference to bregma: AP = −1.2 mm, L = 2 mm, DV = 2.8 mm) according to the atlas of Paxinos and Watson (2005). One week after surgery, rats were randomly assigned for one of the

experimental groups. Drugs were dissolved in DMSO, then using a 5- μ L Hamilton syringe connected to a PE-10 tube, 100 μ g (dissolved in 5 μ L DMSO) of drug was injected over 2 min and the needle remained in place for an additional 1 min before it was slowly retracted. Ten minutes after drug administration, seizure was induced by s.c. injection of freshly prepared PTZ (95 mg/kg) and the animal was observed in a transparent Plexiglas box for 30 min. Seizure severity was measured according to the methods described by Pohl and Mares (1987). These stages are as follow: 1—isolated myoclonic jerks; 2—unilateral and incomplete seizures; 3—clonic seizures; 4—tonic-clonic seizures with a suppression of tonic phase; 5—generalized tonic-clonic seizures. In our study, latency to occurrence for stage 1 and stage 5 of seizure were recorded. These seizure types describe in part absence and generalized tonic-clonic seizure and contribute to different mechanisms of actions of antiseizure drugs. The antiseizure effect of the test compounds was compared with vehicle-treated (control) group and with a standard treatment (carbamazepine 100 μ g).

Whole-cell patch-clamp recording in hippocampal brain slices

Since the hippocampus is an important brain region in seizure development, the hippocampal dentate gyrus (DG) cells were considered for evaluation of the antiseizure mechanism of the effective compound **2a** at 10 μ M concentration.

Brain slice preparation

Rats were deeply anesthetized with i.p. injection of ketamine (100 mg/kg) and xylazine (10 mg/kg) and transcardially perfused with cold (4 °C) modified artificial cerebrospinal fluid (ACSF) containing high sucrose and low sodium (in mM): 206 sucrose, 2.8 KCl, 1.25 NaH₂PO₄, 26 NaHCO₃, 10 glucose, 1 CaCl₂, 2 MgSO₄, 1 MgCl₂, pH = 7.4, oxygenated with 95% O₂ and 5% CO₂. Rats were then decapitated and the brain rapidly removed and placed in the cold sucrose-ACSF solution with the procedure mentioned above. Transverse hippocampal slices (300- μ m thick) were prepared using a vibrating slicer (Campden Instruments Ltd, UK) and transferred to a holding chamber continuously perfused at room temperature with ACSF containing (in mM): 124 NaCl, 3 KCl, 1.24 NaH₂PO₄, 26 NaHCO₃, 10 glucose, 2 CaCl₂, 2 MgSO₄, pH 7.4, oxygenated with 95% O₂ and 5% CO₂.

Whole-cell patch-clamp recording

Whole-cell recordings were done under visual control using infrared difference interference contrast optics. DG granule cells (DG-GCs) were visualized by infrared video imaging (Hamamatsu, ORSA, Japan) with a $\times 40$ water immersion

objective. Whole-cell recordings were made using Multiclamp 700B amplifier (Axon Instruments, CA, USA) equipped with Digidata 1320 A/D converter (Axon Instruments, CA, USA). For the recordings, the patch pipettes were pulled with a PC10 vertical puller (Narishige, Japan) from borosilicate glass capillary (1.2 mm O.D., 0.9 mm I.D. with inner filament). Pipettes had a 3–5 M Ω tip resistance when they were filled with intracellular solution. Recordings were accepted only if the series resistance was <25 M Ω , and if it did not vary by 20% during the experiment. In voltage-clamp recording, the pipettes were filled with a solution containing (in mM); 100 Cs₂MeSO₃, 50 CsCl, 10 HEPES, 1.1 EGTA, 2 Mg-ATP, 0.3 Na₂GTP, 5 QX-314, 5 TEA-Cl, 5 4-AP, and 10 Na₂-Phosphocreatine at pH 7.3 adjusted with CsOH, and the osmolarity of the pipette solution was 290 mOsm. For current-clamp recording, pipettes were filled with intracellular solution containing (in mM) 140 K-Gluconate, 10 HEPES, 2 MgCl₂, 2 Na₂-ATP, 1.1 EGTA, 0.1 CaCl₂, and 0.4 Mg-ATP. The pH of the internal solution was set to 7.3 by KOH, and the osmolarity was adjusted to 290 mOsm. The recordings were filtered by low-pass Bessel at 10 kHz, sampled at 20 kHz and stored on a personal computer for offline analysis. Spontaneous excitatory postsynaptic currents (EPSCs) were recorded in the presence of GABA_A receptor antagonist bicuculline (30 μ M) and were blocked by the ionotropic glutamate receptor antagonists AP-5 (50 μ M) and CNQX (20 μ M). Spontaneous inhibitory postsynaptic currents (IPSCs) were recorded with cesium-containing electrodes in the presence of AP-5 (50 μ M) and CNQX (20 μ M) and were blocked by the GABA_A receptor antagonist bicuculline (30 μ M).

Molecular docking

PDB code 1OHW was used for molecular docking of vigabatrin and **2a** into the active site of GABA-T. Validation of the method was performed by docking of vigabatrin and valproic acid into the active site and comparing the results by a recently reported study on GABA-T inhibitors (Sahu et al. 2018). Docking was performed by AutoDock 4.2 and AutoDock Tools 1.5.6 was used to prepare the protein and the required parameter files. Protonation of the protein and the ligands was performed at pH = 7.4 and the ligands were energy minimized at PM3 level prior to docking calculations. Center of the grid was $X = 9.49$, $Y = -2.656$, $Z = 17.132$, grid spacing was 0.375 and the number of points in the grid was 50, 46, and 50 in each Cartesian coordinates. Lamarckian genetic algorithm was used to search the space and the number of GA runs were set to 20.

Statistical analysis

Data of seizure latency were shown as mean \pm SEM. One-way analysis of variances (ANOVA) followed by Donnet

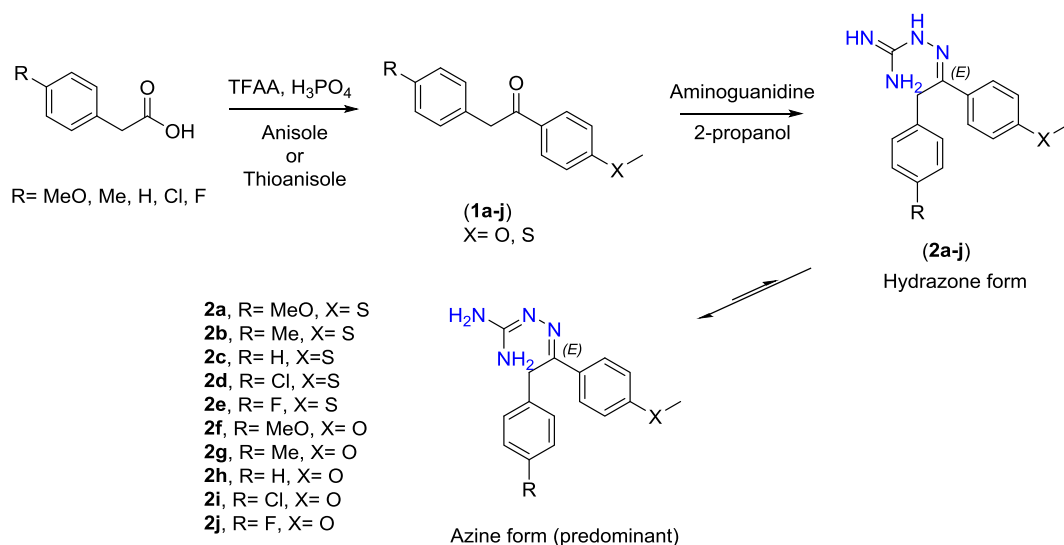
test was used to compare seizure latencies between groups. Also, chi-squared test was used to compare the ratio of seizure occurrence between control and drug-treated groups. Statistical analysis was performed by GraphPad Prism 6.0 (San Diego, CA, USA). P values <0.05 were considered as significant difference.

Results and discussion

Chemistry

Preparation of the target compounds **2a–j**, is outlined in Scheme 1. As presented, synthetic route was started by an acylation-like reaction between phenylacetic acid derivatives and anisole or thioanisole in the presence of trifluoroacetic anhydride and phosphoric acid which has been reported by us in our previous works (Kucukkilinc et al. 2017; Valipour et al. 2019). In the next step, to the 1,2-diarylethanones **1a–j**, was added aminoguanidine in acidic solution of 2-propanol and the mixture was refluxed to give the final products **2a–j**. Target compounds **2a–j** were obtained in pure form by crystallization in 2-propanol. Subsequently, they were accurately characterized by ¹H and ¹³C-NMR as well as mass spectroscopy (spectra in Supplementary material) and the data confirmed their correct structures. In the ¹H-NMR spectra of compounds **2a–j**, a singlet was observed in the range of 4.23–4.34 ppm with integral of two protons which is attributed to the aliphatic methylene (Ar–CH₂–C=N) protons. Methylthio protons in compounds **2a–e**, appeared as a singlet in the range of 2.46–2.47 ppm and protons of methoxy groups (CH₃X in Scheme 1) in compounds **2f–j** are located in the range of 3.75–3.76 ppm. Notably, protons of methoxy groups in the R position of compounds **2a** and **2f** were found in 3.67 ppm. Exchangeable protons attached to nitrogen atoms in hydrazine carboximidamide moiety can be seen as a singlet at a range of 11.54–11.76 and a broad singlet at 7.7–7.8 ppm. Existence of exchangeable protons was confirmed by adding D₂O to the deuterated-DMSO in NMR solution of compound **2i** and observing disappearance of the corresponding signals at their own locations (Fig. 3). ¹³C-NMR spectra of compounds **2a–j** showed that the methylene carbon atoms (Ar–CH₂–C=N) are in the range of 31.3–32.3 ppm, the methylthio carbon atoms at 14.1–14.6 ppm and methoxy carbon atoms (CH₃X–) are in the range of 55.2–55.3 ppm. Imine carbon atoms in the ethylidene moiety of compounds display a signal in the range of 151.8–152.8 ppm and carbon atoms of the guanidine moiety are at the downfield part of the spectrum at the range of 156.0–156.6 ppm.

Due to the presence of the imine bond in the structure of **2a–j**, stereoisomeric *E/Z* forms could be formed during the



Scheme 1 Synthetic route to prepare (*E*)-1,2-diarylethylidenehydrazine carboximidamides **2a-j** and representation of their hydrazone-azine tautomerism

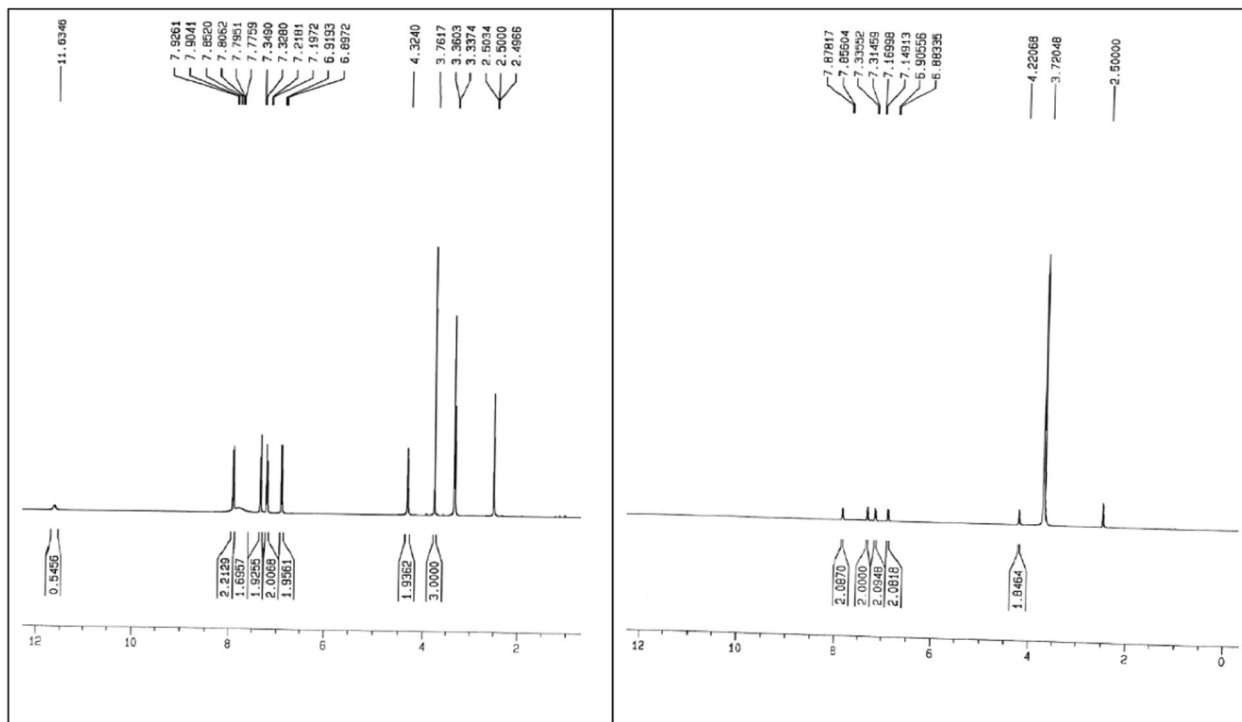


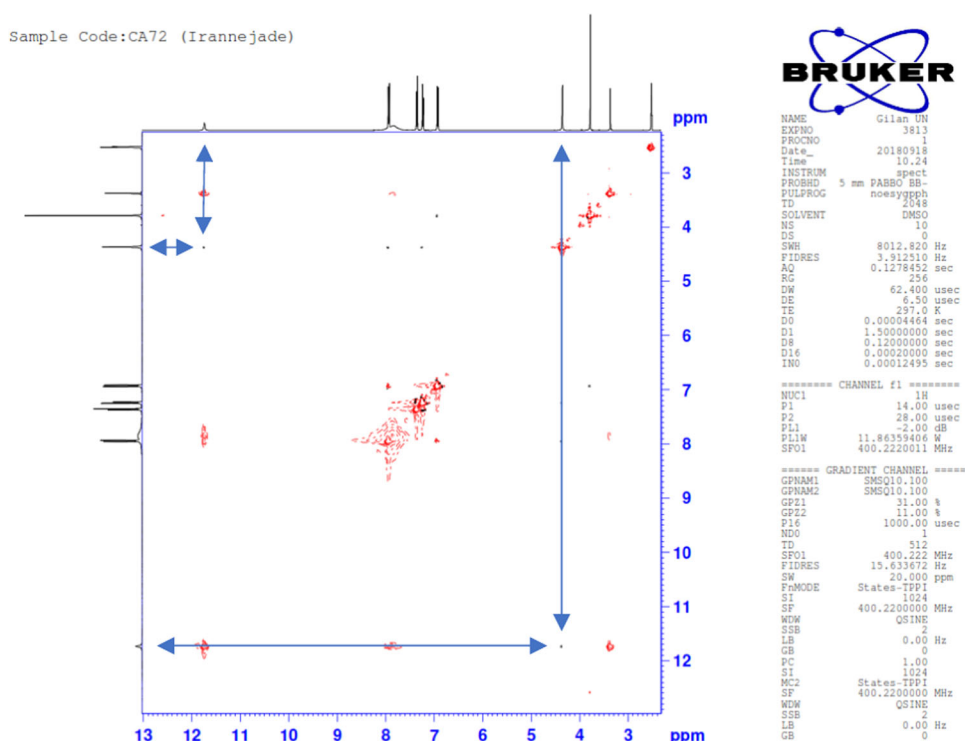
Fig. 3 ^1H -NMR spectrum of compound **2i**. **a** ^1H -NMR spectrum of compound **2i** in DMSO-d_6 . **b** ^1H -NMR spectrum of compound **2i** in a mixture of DMSO-d_6 and D_2O

reaction or after product formation by inversion of the nitrogen atom. Many reports exist in the literature debating and identifying the type and percentage of isomers by ^1H -NMR chemical shifts or by NOE relationships (Dehestani et al. 2018; Silva et al. 2016). The ^1H -NMR spectra of **2a-j** shows that all compounds are in pure isomeric forms because only one peak exists for each proton in the structure. To determine the type of

E/Z isomer of compounds, NOESY assignment was performed for compound **2i** and is shown in Fig. 4. As shown, there is a correlation between methylene protons at 4.36 ppm and guanidine protons at 11.73 ppm and hence confirms the absolute *E*-isomeric form of all compounds.

Hydrazone forms of compounds such as semi-carbazone, thiosemicarbazone, and guanylhyazone

Fig. 4 NOESY spectrum of compound **2i**. Arrows represent the correlation between methylene (CH₂) and guanidine protons



have been used extensively in the literature for the design of new drug-like compounds. But according to quantum and structural studies on these type of compounds, hydrazone-azine tautomerism exists which predominates to the azine formation (Chourasiya et al. 2016). Accordingly, hydrazine carboximidamides **2a–j** are predominantly in the form of azine in which the double bonds are conjugated in the guanylhydrazone moiety as presented in Scheme 1.

The protective effects of **2a–j** against PTZ-induced tonic-clonic and myoclonic seizures

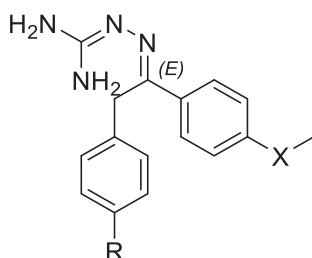
In this study, all tested compounds and carbamazepine as a standard drug were used at a dose of 100 µg/rat and the results were compared with the control group received DMSO as solvent. As shown in Table 1, compounds **2a**, **2c**, **2e**, **2g**, **2h**, **2i**, and **2j** significantly increased latency time to the tonic-clonic seizures compared with the control group ($p < 0.05$) and compounds **2b**, **2d**, and **2f** did not show any protection against tonic-clonic seizures. Accordingly, **2j** had the lowest activity among compounds while compounds **2e** and **2g** showed latency to tonic-clonic seizures with a p value < 0.01 . Interestingly, compounds **2c**, **2h**, and **2i** increased the latency to tonic-clonic seizures with a higher magnitude and a p value < 0.001 . More interestingly, compound **2a** had the highest protection against tonic-clonic seizures with the longest latency time and a p value < 0.0001 which was equipotent as the standard drug carbamazepine.

However, neither the test compounds **2a–j** nor carbamazepine could protect rats against PTZ-induced myoclonic seizures. One-way ANOVA and post tests revealed no significant difference in latency to myoclonic seizure occurrence between groups suggesting no protection against myoclonic seizure with any of the test compounds.

Considering the chemical structure of compounds, the results suggested that the presence of lipophilic atoms or groups in both R and X positions such as **2b** (R = Me, X = S) and **2d** (R = Cl, X = S) diminishes antiseizure activity of compounds. On the other hand, presence of polar groups in the same positions as in **2f** (R = MeO, X = O) also inactivates compounds against seizures control. Therefore, a combination of a polar and a nonpolar group on the two aryl rings confers optimum antiseizure activity. According to the results, lipophilicity seems to play a key role in the antiseizure activity of the compounds. As shown by the calculated lipophilicity values in Table 1, the most lipophilic compounds **2b** and **2d** with logP value of 3.7 and the most polar compound **2f** with logP value of 2.5 are inactive against tonic-clonic seizures. Reasoning of this finding is described in the molecular docking results.

Effects of **2a** in in vivo studies on active and passive properties of hippocampal neurons

In order to explore the possible mechanism of anticonvulsant activity of **2a**, which was very active in behavioral study, it was subjected to electrophysiological investigation to study its

Table 1 Protective effect of pretreatment with carbamazepine and compounds against PTZ-induced tonic-clonic and myoclonic seizures

Compound	Substitution	logP	Tonic-clonic seizure latency (s) (mean ± SEM)	<i>p</i> value ^a	Myoclonic seizure latency (s) (mean ± SEM)	<i>p</i> value
Control (DMSO)	–	–	458 ± 63	–	161 ± 19	–
2a	R = MeO, X = S	3.1	1800 ± 0	<i>p</i> < 0.0001	360 ± 90	NS
2b	R = Me, X = S	3.7	1092 ± 297	NS	228 ± 51	NS
2c	R = H, X = S	3.2	1548 ± 209	<i>p</i> < 0.001	216 ± 40	NS
2d	R = Cl, X = S	3.7	1170 ± 134	NS	384 ± 52	NS
2e	R = F, X = S	3.3	1428 ± 209	<i>p</i> < 0.01	315 ± 66	NS
2f	R = MeO, X = O	2.5	941 ± 244	NS	564 ± 236	NS
2g	R = Me, X = O	3.1	1450 ± 245	<i>p</i> < 0.01	791 ± 319	NS
2h	R = H, X = O	2.6	1620 ± 180	<i>p</i> < 0.001	642 ± 253	NS
2i	R = Cl, X = O	3.2	1574 ± 226	<i>p</i> < 0.001	535 ± 316	NS
2j	R = F, X = O	2.8	1249 ± 278	<i>p</i> < 0.05	521 ± 320	NS
Carbamazepine	–	–	1800 ± 0	<i>p</i> < 0.0001	302 ± 49	NS

The antiseizure effect of drugs (100 µg/5 µL vehicle; i.c.v. administration) in PTZ-induced seizure in rats

Drugs (100 µg/rat) or DMSO (in control group) were microinjected (5 µl) into left lateral ventricle 15 min before s.c. administration of PTZ (95 mg/kg). After PTZ injection, rats were monitored for 30 min for seizure occurrence (cutoff point 1800s). *N* = 6–8 per group

NS not significant

^aStatistically significant compared with the control (DMSO) group

effects on electrophysiological properties of DG neurons in rat hippocampus.

Current-clamp studies: effect of bath application of 2a on active and passive properties of membrane ion channels in DG hippocampal neurons

Basically, DG-GCs had an initial membrane conductance of 0.27 ± 0.05 pS and bath application of **2a** did not significantly change the membrane conductance (0.39 ± 0.13 pS; Fig. 5). Depolarizing currents-induced neuronal excitability as shown in Fig. 6 by increased number of action potential and eventually inactivation of sodium channels. Two-way ANOVA showed no significant effect of **2a** on the number of action potentials before and after bath application of **2a** [$F(1,39) = 0.3764$; $p = 0.543$] suggesting no blocking effect of **2a** on voltage-gated sodium channels. Moreover, bath application of **2a** did not change rheobase current and utilization time compared with the baseline (Fig. 7). The rheobase current (minimal required current to induce action potential)

changed from 77.56 ± 12.8 pA at the baseline to 76.12 ± 13.37 pA after bath application of **2a**. Similarly, the utilization time (latency to the first action potential in Ramp test) changed from 381.6 ± 63.47 ms at the baseline to 377.75 ± 63.9 ms after bath application of **2a**.

A change in AHP (after hyperpolarization) could suggest the effect of **2a** on calcium-activated potassium channels, which is important in seizure treatment. As shown in Fig. 8, no significant effect of treatment on AHP amplitude was shown in different steps of depolarizing currents [$F(1,33) = 4.114$; $p = 0.05$], although a slight increase in AHP was detected after bath application of **2a**.

Voltage-clamp studies: effect of bath application of 2a on excitatory and inhibitory synaptic transmission in DG hippocampal neurons

In order to evaluate the effects of **2a** on synaptic transmission of DG hippocampal neurons, the inter-event intervals (IEI) and amplitude of IPSCs and EPSCs were determined at baseline values and after bath application of **2a**. As shown in

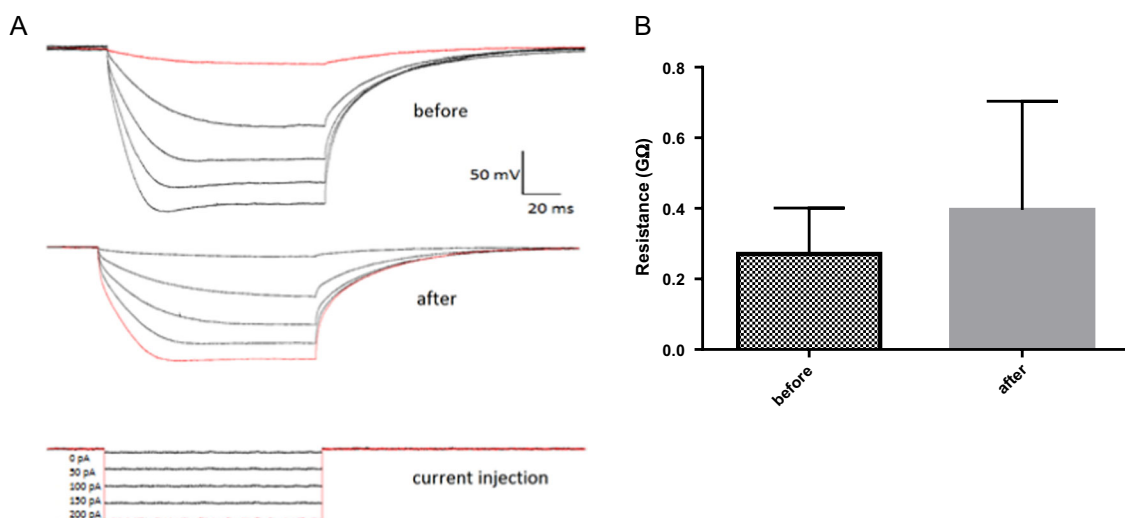


Fig. 5 **a** Representative traces and relative current–voltage (I – V) curve obtained by applying hyperpolarizing currents to DG cells. The slope of the fitted line represents total resistance of the cell membrane.

b Average of membrane resistance before and after bath application of **2a** shows no significant effect of the drug on membrane resistance. Data were shown as mean \pm SEM ($n = 5$)

Fig. 9a, for IPSCs, a left shift in cumulative histogram of IEI in a DG neuron suggested a decrease in IEI or an increase in the number of IPSCs. Paired t -test revealed a significant decrease in IEI ($p = 0.027$) but no change in IPSCs amplitude compared with the baseline values, suggesting a possible presynaptic augmentation of inhibitory neurotransmission by **2a**. Moreover, **2a** caused a right shift in cumulative histogram of IEI for EPSCs with no change in amplitude (Fig. 10a). Also, paired t -test revealed a significant increase in IEI of EPSCs ($p < 0.05$) but no change in EPSCs amplitude compared with the baseline values (Fig. 10b), suggesting a possible presynaptic inhibition of EPSCs by **2a** in DG neurons.

Accordingly, it is believed that **2a** might act through the inhibition of GABA-transaminase (GABA-T) to exert its antiseizure activity. Since this enzyme is one of the main targets for some well-known anticonvulsant drugs like vigabatrin and valproic acid, **2a** was further considered for docking into the active site of GABA-T as a potential target for (*E*)-1,2-diarylethylidenehydrazine carboximidamides.

Molecular docking study

According to the results obtained by the electrophysiological patch-clamp study, the possible mechanism of action of (*E*)-1,2-diarylethylidenehydrazine carboximidamide **2a** was suspected to be through the inhibition of GABA-T. This enzyme degrades the inhibitory neurotransmitter GABA to end its physiological action and its inhibition increases the synaptic concentration of GABA.

To model the binding strength of **2a** and its hypothetical interactions with the key residues in the active site of GABA-T, molecular docking is a reliable and useful tool for medicinal chemists. Since the PDB structure of the X-ray

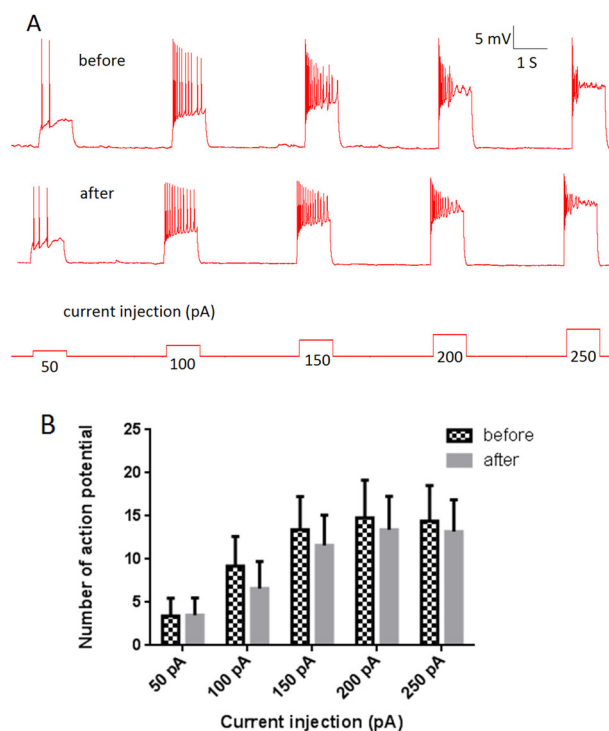


Fig. 6 **a** could not alter depolarizing currents-induced action potential properties. **a** Representative traces and **b** average of the number of action potentials at different depolarizing currents show no change after bath application of **2a** compared with the baseline values. Data were shown as mean \pm SEM ($n = 5$)

crystallized Homo sapiens GABA-T is not available yet, the PDB code 1OHW which is the Sus scrofa GABA-T can be used for molecular docking. According to a recent study on GABA-T inhibitors, human GABA-T (UniProt id-P80404) has 95.2% sequence identity with the Sus scrofa (UniProt id-P80147) and the active site residues are highly conserved

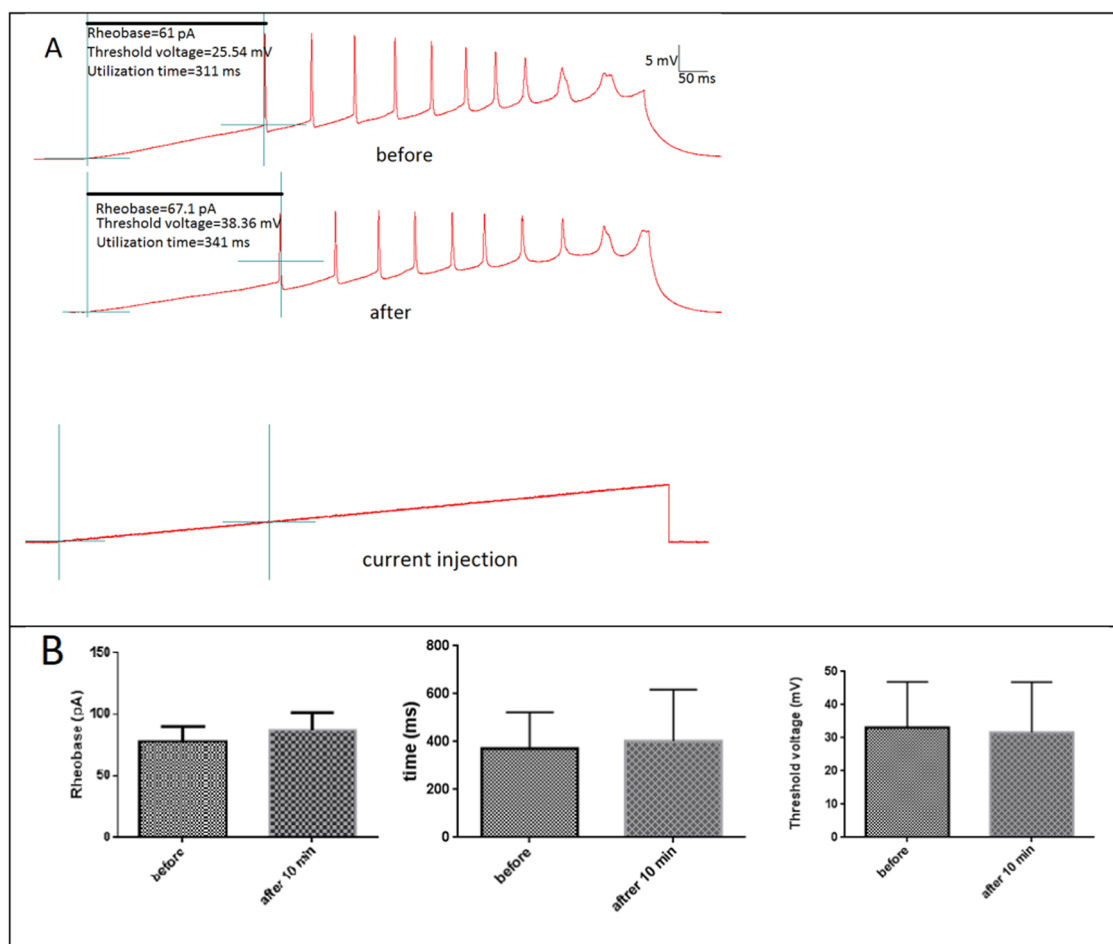


Fig. 7 Effect of **2a** on membrane excitability of DG cells in Ramp test. **a** Representative trace showing the minimum current of electrical stimulus to excite the membrane (rheobase), the time taken by a stimulus of rheobase strength to excite the membrane (utilization time),

and the threshold voltage. **b** No change in rheobase, utilization time, or threshold voltage were shown after bath application of **2a** compared with the baseline values. Data were shown as mean ± SEM ($N = 5$)

(>96%), therefore PDB code 1OHV can be used with confidence (Sahu et al. 2018).

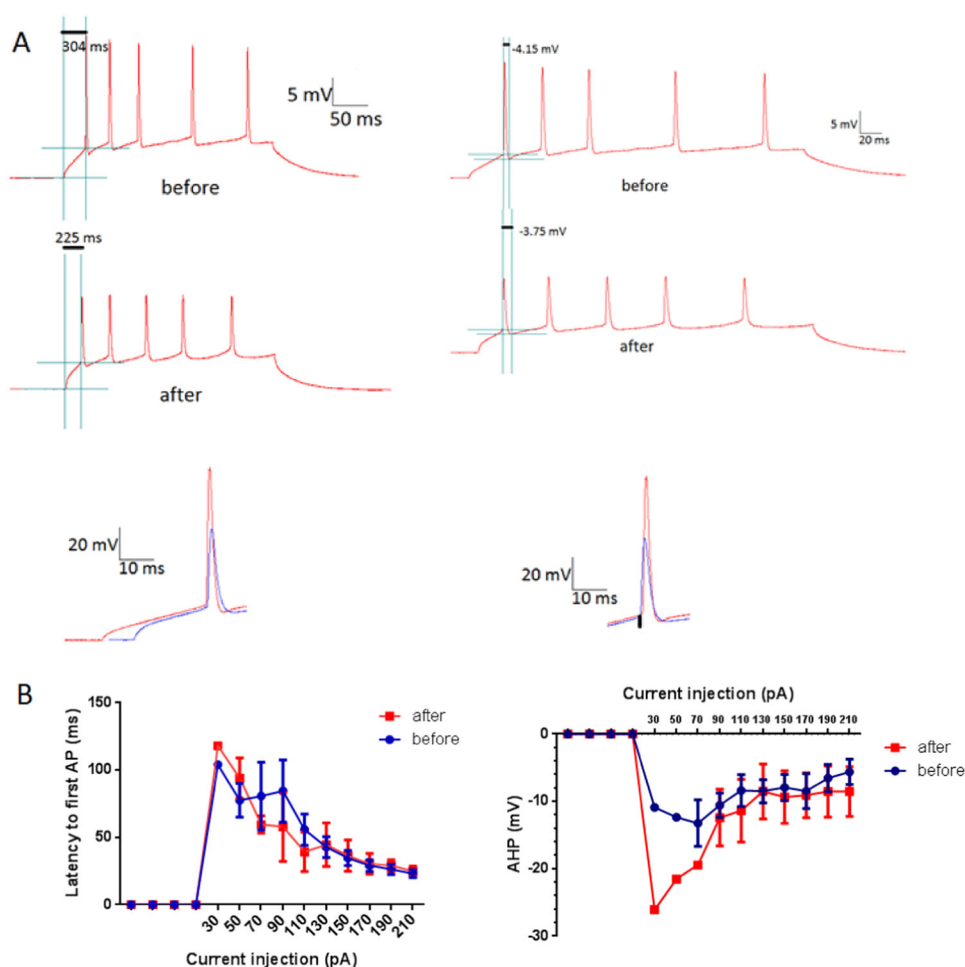
Basically, the enzyme exists in a tetrameric form and its active site is located at the interface of the two monomer including the residues surrounding the pyridoxal phosphate (PLP). Correspondingly, **2a** in its azine form and vigabatrin as a standard GABA-T inhibitor were subjected to molecular docking into the active site of the enzyme.

The calculated binding energy was found to be -3.08 kcal/mol for vigabatrin while **2a** showed better binding energy (-5.56 kcal/mol) and higher affinity than vigabatrin into the active site of the enzyme. The conformational binding mode and interactions of **2a** and vigabatrin in the active site of GABA-T are illustrated in Fig. 11. In the case of **2a**, phenyl ring of the 4-methylthiophenyl, has pi-pi T-shaped interactions with Phe189A (4.77 Å) and its methylthio group has pi-alkyl and pi-sulfur interactions with the phenyl ring of Phe351B (5.13 and 4.52 Å, respectively). Likewise, the other phenyl ring in the 4-

methoxyphenyl, has pi-donor or arene-H interactions with amide NH of Gly136A (2.92 Å) and Thr353B (3.22 Å) as well as a pi-alkyl interaction with Cys135A (4.06 Å). Correspondingly, amidine NH of **2a** has conventional hydrogen bonds with carbonyl oxygen of Phe189A (2.05 Å) and carboxylate group of Asp298A (1.78 and 2.92 Å) (Fig. 11). Similarly, hydrazone form of **2a** produced very similar results to the azine form in binding energy and conformation in the docking calculations.

Likewise, carboxylate oxygen atom of vigabatrin has hydrogen bonding to the NH of Gln301A (1.96 Å) and amine group of Lys329A (2.12 Å). Correspondingly, ammonium group of vigabatrin has two attractive ionic interactions with Glu265A and Glu299A (3.84 Å) and conventional hydrogen bonding to the carboxylate group of Asp298A (1.74 Å). Similarly, the binding conformation of vigabatrin has located in the same space as predicted by a previously reported study on GABA-T inhibitors and have Lys329A and Gln301A as common interacting residues (Sahu et al. 2018).

Fig. 8 Effect of bath application of **2a** on latency to first action potential (left) and AHP amplitude (right) in DG cells. Representative traces (**a**) and average of data (**b**) show no significant change in either latency to first action potential or AHP amplitude after drug application compared with the baseline values. Data were shown as mean \pm SEM ($N = 5$)



As noted earlier in the *in vivo* results, for the optimum antiseizure activity of compounds, one of the aromatic rings has to bear a lipophilic moiety while the other ring must contain a polar group. This fact was further confirmed by presenting the surface hydrophobicity of GABA-T active site residues in Fig. 12. As illustrated, the methylthio group of **2a** is located into a more hydrophobic space (brown color) due to the presence of Phe351 and Phe189 than the methoxy group. This finding confirms that compounds which have hydrophobic groups on the both of the two aryl rings (**2b** and **2d**) or the ones which have polar groups on the both of them (**2f**) cannot accommodate well into the GABA-T active site and hence will be inactive.

Prediction of ADME parameters

Prediction of the druglikeness and ADME properties of compound **2a** were calculated by admetSAR 2.0 web-service (Yang et al. 2018) and is summarized in Table 2. As shown in the Table, **2a** has no violation of Lipinski's Rule of Five and all the parameters of druglikeness are in the normal range.

Interestingly, **2a** has acceptable Human Intestinal Absorption, Caco-2 permeability and blood–brain barrier penetration. However, it has poor oral bioavailability predicted by this web-server probably due to its high hepatic clearance. On the other hand, **2a** is neither a P-glycoprotein (P-gp) substrate nor a P-gp inhibitor and hence does not have drug resistance due to P-gp efflux. Correspondingly, **2a** was predicted to be an inhibitor of CYP3A4 and substrate of CYP2D6 which are the factors affecting its low oral bioavailability.

Conclusion

(*E*)-1,2-Diarylethylidenehydrazine carboximidamides as new anticonvulsant agents were synthesized and characterized by NOESY experiment to confirm their (*E*)-stereoisomeric form. Evaluation of their antiseizure activity by *i.c.v.* administration showed their prominent activity against tonic-clonic seizures. Correspondingly, **2a** was found to be the most potent one as equipotent as carbamazepine in controlling the seizures. Patch-clamp results confirmed that **2a** is neither a voltage-gated

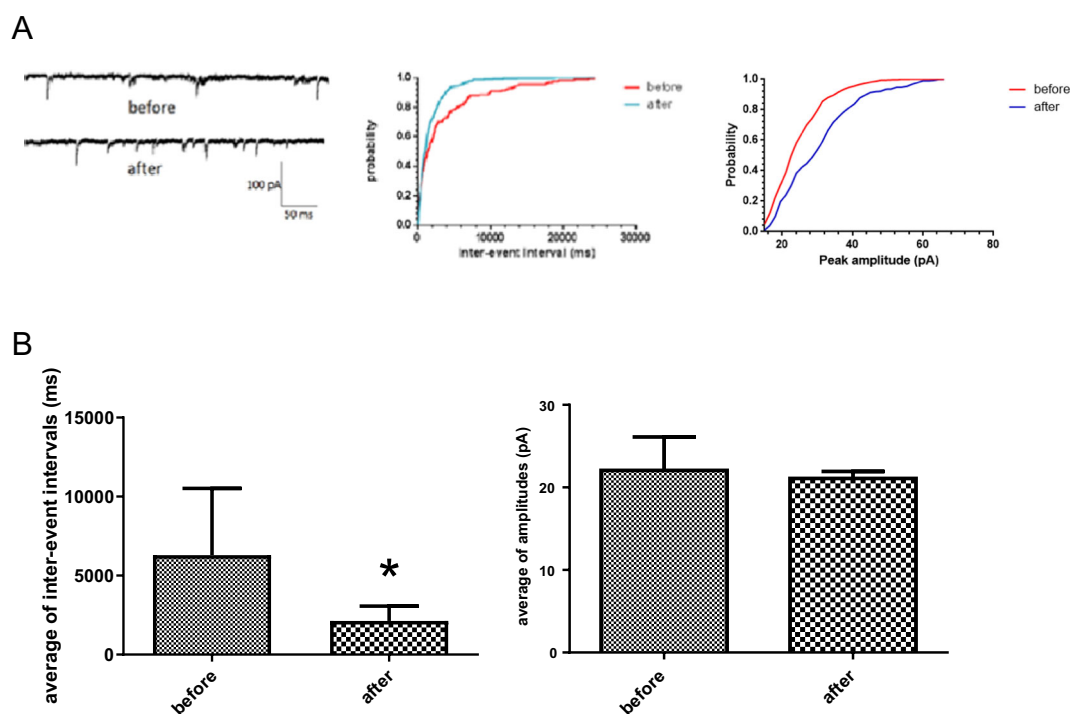


Fig. 9 **2a** increased IPSCs frequency with no change in IPSCs amplitude. **a** Representative IPSCs and the cumulative histograms of inter-event interval (IEI) and amplitude of the same cell. Bath application of **2a** could shift the histogram to the left (i.e. a decrease in IEIs)

with no change in IPSCs amplitude. **b** Bath application of **2a** significantly increased the number of IPSCs during 10 min of recording compared with the baseline values. Data were shown as mean \pm SEM ($N = 5$). $*p < 0.05$ (paired t -test)

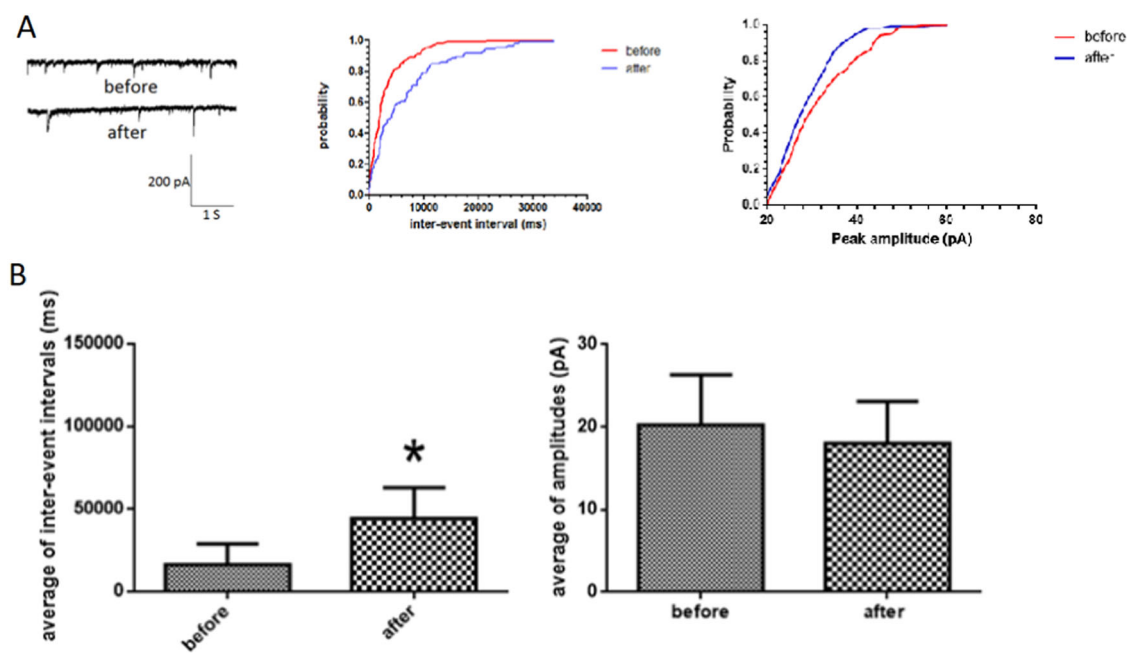
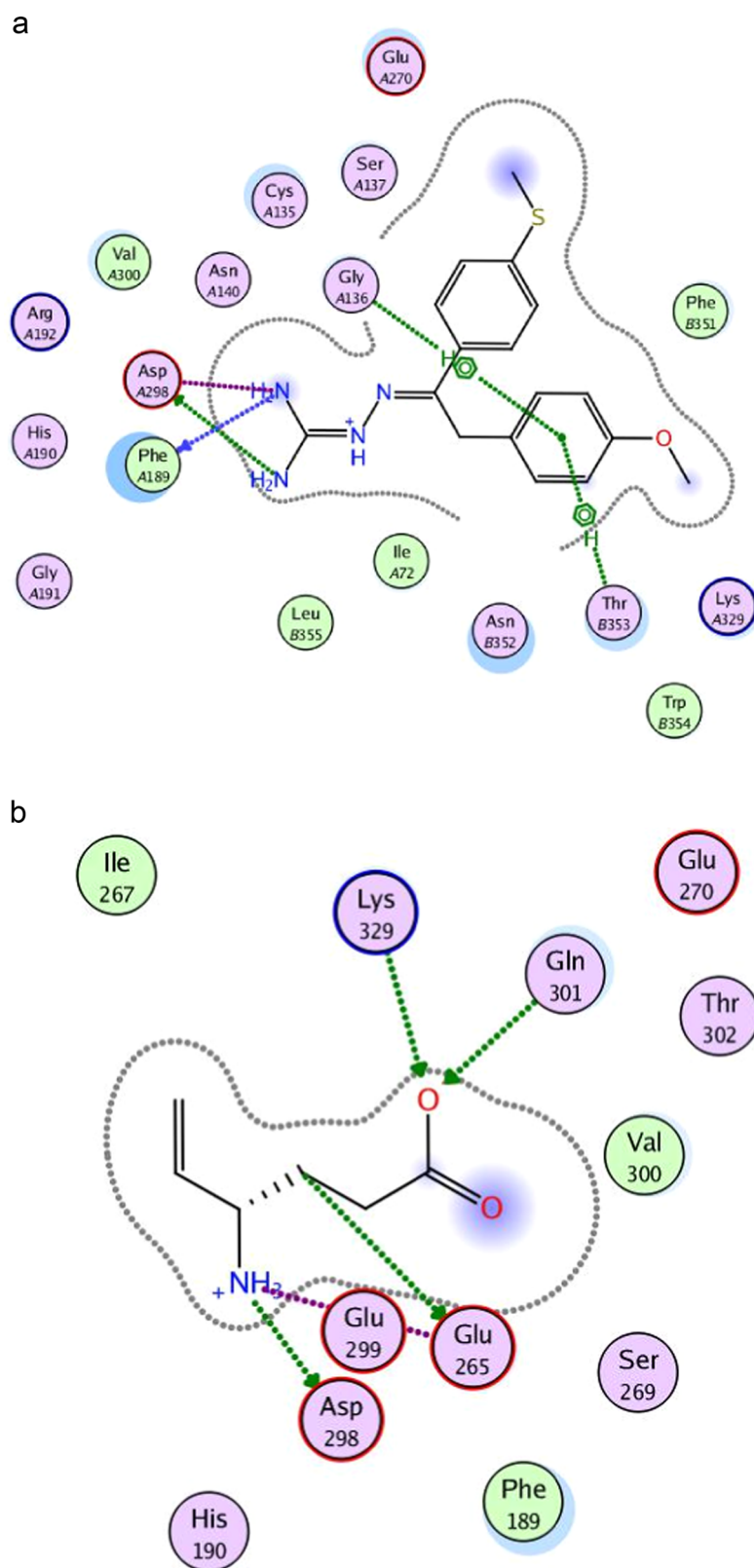


Fig. 10 **2a** decreased EPSCs frequency with no change in EPSCs amplitude. **a** Representative EPSCs and the cumulative histograms of inter-event interval (IEI) and amplitude of the same cell. Bath application of **2a** could shift the histogram to the right (i.e. an increase in IEIs) with no change in amplitude. **b** Bath application of **2a**

significantly increased inter-event intervals of EPSCs during 10 min of recording compared with the baseline values while no change in EPSCs amplitude. Data were shown as mean \pm SEM ($N = 5$). $*p < 0.05$ (paired t -test)

Fig. 11 2D map of the binding conformation and interactions of (a) **2a** and (b) vigabatrin in the active site of GABA-T



sodium channel blocker, nor an AMPA or NMDA antagonist. Besides, **2a** did not induce any direct GABA

current but could decrease EPSP and increase IPSP frequency without any change in amplitude. Totally, the

Fig. 12 Surface hydrophobicity presentation of the GABA-T active site residues

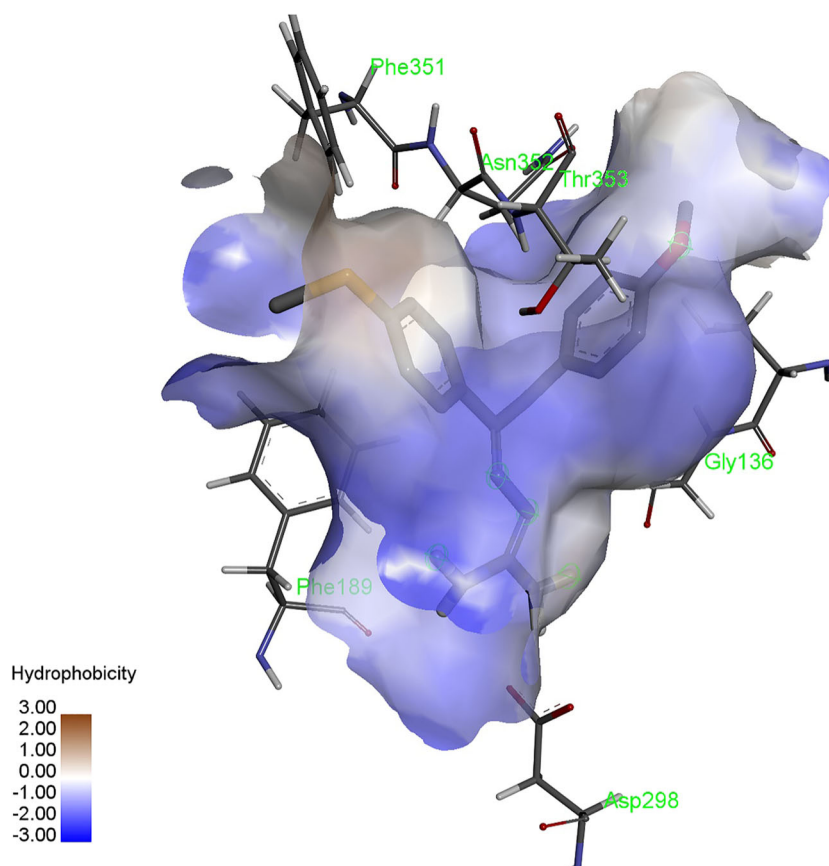


Table 2 Physicochemical parameters and ADME profile of compound **2a** predicted by admetSAR 2.0 web-service

Parameter	Value	Parameter	Value	Parameter	Value
Molecular weight	328.44	Human intestinal absorption	Yes	CYP3A4 substrate	No
AlogP	2.85	Caco-2	Yes	CYP2C9 substrate	No
H-bond acceptor	4	Blood–brain barrier	Yes	CYP2D6 substrate	Yes
H-bond donor	3	Human oral bioavailability	No	CYP3A4 inhibitor	Yes
Rotatable bonds	6	P-glycoprotein inhibitor	No	CYP2C9 inhibitor	No
Applicability domain	Yes	P-glycoprotein substrate	No	CYP2D6 inhibitor	No

results guided us to conclude a presynaptic mechanism of **2a** for its antiseizure activity and prompted us to consider GABA-T as a probable target for (*E*)-1,2-Diarylethylidenehydrazine carboximidamides.

Acknowledgements This work was supported in part by a grant from Mazandaran University of Medical Sciences (grant No. 1796) and also by grant from Shahid Beheshti University of Medical Sciences (grant No. 9487).

Compliance with ethical standards

Conflict of interest The authors declare that they have no conflict of interest.

Publisher's note Springer Nature remains neutral with regard to jurisdictional claims in published maps and institutional affiliations.

References

- Arshia A, Khan A, Khan KM, Saad SM, Siddiqui NI, Javaid S, Choudhary MI (2016) Synthesis and urease inhibitory activities of benzophenone semicarbazones/thiosemicarbazones. *Med Chem Res* 25(11):2666–2679
- Chourasiya SS, Kathuria D, Nikam SS, Ramakrishnan A, Khullar S, Mandal SK, ... Bharatam PV (2016) Azine-hydrazone tautomerism of guanylhya zones: evidence for the preference toward the azine tautomer. *J Org Chem* 81(17): 7574–7583. <https://doi.org/10.1021/acs.joc.6b01258>

- Dehestani L, Ahangar N, Hashemi SM, Irannejad H, Honarchian Masihi P, Shakiba A, Emami S (2018) Design, synthesis, in vivo and in silico evaluation of phenacyl triazole hydrazones as new anticonvulsant agents. *Bioorg Chem* 78: 119–129. <https://doi.org/10.1016/j.bioorg.2018.03.001>
- Fatondji HR, Kpoviessi S, Gbaguidi F, Bero J, Hannaert V, Quetin-Leclercq J, Accrombessi GC (2013) Structure–activity relationship study of thiosemicarbazones on an African trypanosome: *trypanosoma brucei brucei*. *Med Chem Res* 22(5):2151–2162
- Haldys K, Goldeman W, Jewginski M, Wolinska E, Anger N, Rosowska J, Latajka R (2018) Inhibitory properties of aromatic thiosemicarbazones on mushroom tyrosinase: Synthesis, kinetic studies, molecular docking and effectiveness in melanogenesis inhibition. *Bioorg Chem* 81: 577–586. <https://doi.org/10.1016/j.bioorg.2018.09.003>
- Irannejad H, Naderi N, Emami S, Ghadikolaei RQ, Foroumadi A, Zafari T, Dadashpour S (2014) Microwave-assisted synthesis and anticonvulsant activity of 5,6-bisaryl-1,2,4-triazine-3-thiol derivatives. *Med Chem Res* 23(5):2503–2514. <https://doi.org/10.1007/s00044-013-0843-6>
- Irannejad H, Nadri H, Naderi N, Rezaeian SN, Zafari N, Foroumadi A, Khoobi M (2015) Anticonvulsant activity of 1,2,4-triazine derivatives with pyridyl side chain: synthesis, biological, and computational study. *Med Chem Res* 24(6):2505–2513. <https://doi.org/10.1007/s00044-014-1315-3>
- Kucukkılinc TT, Yangghagh KS, Ayazgok B, Roknipoor MA, Moghadam FH, Moradi A, Irannejad H (2017) Synthesis and neuroprotective activity of novel 1, 2, 4-triazine derivatives with ethyl acetate moiety against H₂O₂ and A β -induced neurotoxicity. *Med Chem Res* 26(11):3057–3071
- Kumar GD, Chavarria GE, Charlton-Sevcik AK, Yoo GK, Song J, Strecker TE,... Pinney KG (2010) Functionalized benzophenone, thiophene, pyridine, and fluorene thiosemicarbazone derivatives as inhibitors of cathepsin L. *Bioorg Med Chem Lett* 20(22):6610–6615. <https://doi.org/10.1016/j.bmcl.2010.09.026>
- Nevagi RJ, Dhake AS, Narkhede HI, Kaur P (2014) Design, synthesis and biological evaluation of novel thiosemicarbazide analogues as potent anticonvulsant agents. *Bioorg Chem* 54:68–72. <https://doi.org/10.1016/j.bioorg.2014.04.002>
- Paxinos G, Watson C (2005) The rat brain in stereotaxic coordinates, 5th edn. Academic Press, New York
- Pelosi G, Bisceglie F, Bignami F, Ronzi P, Schiavone P, Re MC,... Pilotti E (2010) Antiretroviral activity of thiosemicarbazone metal complexes. *J Med Chem* 53(24):8765–8769. <https://doi.org/10.1021/jm1007616>
- Perucca E, Meador KJ (2005) Adverse effects of antiepileptic drugs. *Acta Neurol Scand Suppl* 181:30–35. <https://doi.org/10.1111/j.1600-0404.2005.00506.x>
- Pitucha M, Woś M, Miazga-Karska M, Klimek K, Mirosław B, Pachuta-Stec A, Ginalska G (2016) Synthesis, antibacterial and antiproliferative potential of some new 1-pyridinecarbonyl-4-substituted thiosemicarbazide derivatives. *Med Chem Res* 25(8):1666–1677
- Pohl M, Mares P (1987) Effects of flunarizine on Metrazol-induced seizures in developing rats. *Epilepsy Res* 1(5):302–305. [https://doi.org/10.1016/0920-1211\(87\)90006-4](https://doi.org/10.1016/0920-1211(87)90006-4)
- Sahu M, Siddiqui N, Sharma V, Wakode S (2018) 5,6-Dihydropyrimidine-1(2H)-carbothioamides: Synthesis, in vitro GABA-AT screening, anticonvulsant activity and molecular modelling study. *Bioorg Chem* 77:56–67. <https://doi.org/10.1016/j.bioorg.2017.12.031>
- Shafiee A, Rineh A, Kebriaeezadeh A, Foroumadi A, Sheibani V, Afarinesh MR (2009) Synthesis and anticonvulsant activity of 4-(2-phenoxyphenyl) semicarbazones. *Med Chem Res* 18(9):758
- Silva FT, Franco CH, Favaro DC, Freitas-Junior LH, Moraes CB, Ferreira EI (2016) Design, synthesis and antitrypanosomal activity of some nitrofurazone 1,2,4-triazolic bioisosteric analogues. *Eur J Med Chem* 121:553–560. <https://doi.org/10.1016/j.ejmech.2016.04.065>
- Song S, You A, Chen Z, Zhu G, Wen H, Song H, Yi W (2017) Study on the design, synthesis and structure-activity relationships of new thiosemicarbazone compounds as tyrosinase inhibitors. *Eur J Med Chem* 139:815–825. <https://doi.org/10.1016/j.ejmech.2017.08.033>
- Tripathi L, Kumar P (2013) Augmentation of GABAergic neurotransmission by novel N-(substituted)-2-[4-(substituted)benzylidene]hydrazinecarbothioamides-a potential anticonvulsant approach. *Eur J Med Chem* 64:477–487. <https://doi.org/10.1016/j.ejmech.2013.04.019>
- Valipour M, Davaji I, Abedi N, Rajabi M, Tüylü Küçükkılınç T, Ayazgök B, Irannejad H (2019) Synthesis and biological assessment of 2-hydroxyiminoethanones as anti-inflammatory and β -amyloid aggregation inhibitors. *Iran J Pharm Res* 18(3):1288–1298
- Yang H, Lou C, Sun L, Li J, Cai Y, Wang Z, Tang Y (2018) admetSAR 2.0: web-service for prediction and optimization of chemical ADMET properties. *Bioinformatics* 35(6):1067–1069. <https://doi.org/10.1093/bioinformatics/bty707>